

THE EFFECT OF THE ENSKOG COLLISION TERMS ON THE STEADY SHOCK STRUCTURE IN A HARD SPHERE GAS

RAFAIL V. ABRAMOV

ABSTRACT. In this work we study the effect of the Enskog collision terms on the steady shock transitions in the supersonic flow of a hard sphere gas. We start by examining one-dimensional, nonlinear, nondispersive planar wave solutions of the Enskog–Navier–Stokes equations, which move in a fixed direction at a constant speed. By further equating the speed of the reference frame with the speed of such a wave, we reduce the Enskog–Navier–Stokes equations into a more simple system of two ordinary differential equations, whose solutions depend on a single scalar spatial variable. We then observe that this system has two fixed points, which are taken to be the states of the gas before and after the shock, and compute the corresponding shock transition in the form of the heteroclinic orbit connecting these two states. We find that the Enskog correction affects both the difference between the fixed points, and the thickness of the transition. In particular, for a given state of the gas before the shock transition, the difference between the fixed points is reduced, while the shock thickness is increased, with the relative impact on the properties of transition being more prominent at low Mach numbers. We also compute the speed of sound in the Enskog–Navier–Stokes equations, and find that, for the same thermodynamic state, it is somewhat faster than that in the conventional Navier–Stokes equations, with an additional dependence on the density of the gas.

1. INTRODUCTION

Conventionally, the hard sphere gas is modeled by the famous Boltzmann equation [7, 12–14]. The corresponding fluid dynamics approximation is given by the Navier–Stokes equations [5, 27]. This conventional theory is used in many engineering applications, and is a good approximation for gases at normal conditions (that is, not too rarefied, and not too dense).

However, in a number of works [9–11, 16, 18, 19, 29] it was noted that, in certain situations, the conventional model, offered via the Boltzmann equation and the Navier–Stokes equations, failed to capture some features of the flow of a real gas. In particular, in [29] it was observed that the shock transition thickness in a real gas was not captured accurately by the conventional Navier–Stokes equations; the latter produced a much thinner shock transition than what was actually observed. It was speculated in [9–11, 16, 18, 19, 36, 40] that an *ad hoc* diffusive term could mitigate some of the discrepancies between the observed and modeled behavior. In [1, 3] we studied a diffusive higher-order approximation to the gas dynamics, based on the Grad moment truncation [28, 41].

DEPARTMENT OF MATHEMATICS, STATISTICS AND COMPUTER SCIENCE, UNIVERSITY OF ILLINOIS AT CHICAGO, 851 S. MORGAN ST., CHICAGO, IL 60607

E-mail address: abramov@uic.edu.

In [2], we proposed a new model of the hard sphere gas, based on random interactions. This model consists of a random jump process [4,17,23,39], whose infinitesimal generator [15] allows a straightforward construction of the forward Kolmogorov equation for the probability density of states of the full multi-sphere system. We found a physically realistic family of the steady states, and, with its help, constructed the forward equation for the marginal statistical distribution of a single sphere. This equation turned out to be the Enskog equation [21], originally obtained by Enskog as an *ad hoc* model of a dense gas. In [25], it was found that the Enskog equation produced accurate shock transitions for a wide range of regimes.

In addition to the new random hard sphere model, in [2] we proposed a new hydrodynamic limit, where the density of each sphere of gas is kept constant while its diameter becomes small. This limit is different from the conventional Boltzmann–Grad limit [28], and appears to be more realistic for noble gases. In the constant-density limit, we found that the resulting Enskog–Euler [37] and Enskog–Navier–Stokes equations acquire additional corrections, both in the advective and viscous terms. In the present work, we study the shock transitions produced by the Enskog–Navier–Stokes equations [2], and compare them with those produced by the conventional Navier–Stokes equations [5,27].

1.1. The Enskog–Navier–Stokes equations. In [2], we derived the Enskog–Navier–Stokes equations for the hard sphere gas. What follows is a rough sketch of the procedure of derivation:

- (1) We found that the conventional derivation [14] of the Boltzmann equation had logical inconsistencies. In particular, we observed that solutions of the Boltzmann equation violated assumptions, under which the latter was derived (see Section 3 of [2] for more details).
- (2) However, the Boltzmann equation is known to be a very accurate model of a gas, which means that the equation itself is valid, even though its conventional derivation is flawed. To this end, we introduced a mathematically consistent model of the hard sphere gas, which uses a random jump process with conditional intensity [4,17,22,39] at its foundation (see Section 4 of [2] for more details).
- (3) The Bogoliubov–Born–Green–Kirkwood–Yvon formalism [6,8,35], applied to the random hard sphere model in [2], yields a variant of Enskog equation [34] for K spheres in the form

$$(1.1) \quad \frac{\partial f}{\partial t} + \mathbf{v} \cdot \frac{\partial f}{\partial \mathbf{x}} = (K-1)\sigma^2 R(\sigma) \int \mathbf{n} \cdot (\mathbf{w} - \mathbf{v}) \Theta(\mathbf{n} \cdot (\mathbf{w} - \mathbf{v})) [f(\mathbf{x}, \mathbf{v}')f(\mathbf{x} + \sigma\mathbf{n}, \mathbf{w}') - f(\mathbf{x}, \mathbf{v})f(\mathbf{x} - \sigma\mathbf{n}, \mathbf{w})] d\mathbf{n} d\mathbf{w}.$$

Above, $f(t, \mathbf{x}, \mathbf{v})$ is the probability density of distribution of a single molecule over the velocities and coordinates (same as in the Boltzmann equation), σ is the diameter of a sphere, \mathbf{n} is a vector on a unit sphere, while $\Theta(x)$ is the usual Heaviside function. In the collision integral, the recedent velocities \mathbf{v}' and \mathbf{w}' are given via the usual deflection formulas [12–14]

$$(1.2) \quad \mathbf{v}' = \mathbf{v} + ((\mathbf{w} - \mathbf{v}) \cdot \mathbf{n})\mathbf{n}, \quad \mathbf{w}' = \mathbf{w} + ((\mathbf{v} - \mathbf{w}) \cdot \mathbf{n})\mathbf{n}.$$

The main difference between the collision integrals of the conventional Enskog equation (see, e.g. Eqn. (9.3-6) in [34], or Eqn. (1) in either [24] or [25]) and those of the random hard sphere Enskog equation in (1.1) and [2] is that the collision integral of the former contains an empirical factor obtained via the virial expansion of the equation of state of the gas (see Eqn. (9.3-2) in [34]), while the collision integral of (1.1) is prepended by the spatial correlation function $R(\sigma)$. This correlation function is the result of the systematic closure of the joint two-particle distribution via two single-particle distributions, and the exact expression for $R(\sigma)$ is given by the Eqn. (146) in [2]. As a result, the gas is not required to be *dilute* in the Enskog equation (1.1), that is, the distances between the spheres are not required to be much larger than their diameters, and the spheres themselves are no longer presumed to be distributed statistically independently. See Section 6 in [2] for more details on the derivation of the Enskog equation in (1.1).

- (4) In order to derive the Enskog–Navier–Stokes equations, the probability density in (1.1) must be weighted by the total mass of the system of K spheres. To account for that, in [2] we endowed each sphere with mass density ρ_{sp} , and introduced the mass-weighted probability distribution

$$(1.3) \quad g(t, \mathbf{x}, \mathbf{v}) = Km f(t, \mathbf{x}, \mathbf{v}), \quad m = \frac{1}{6} \pi \rho_{sp} \sigma^3.$$

Substituting the expression for g into (1.1), and taking the number of spheres $K \rightarrow \infty$, in [2] we arrived at the mass-weighted Enskog equation:

$$(1.4) \quad \frac{\partial g}{\partial t} + \mathbf{v} \cdot \frac{\partial g}{\partial \mathbf{x}} = \frac{6R(\sigma)}{\pi \rho_{sp} \sigma} \int \mathbf{n} \cdot (\mathbf{w} - \mathbf{v}) \Theta(\mathbf{n} \cdot (\mathbf{w} - \mathbf{v})) [g(\mathbf{x}, \mathbf{v}') g(\mathbf{x} + \sigma \mathbf{n}, \mathbf{w}') - g(\mathbf{x}, \mathbf{v}) g(\mathbf{x} - \sigma \mathbf{n}, \mathbf{w})] d\mathbf{n} d\mathbf{w}.$$

- (5) Recall that the conventional Navier–Stokes equations are obtained from the Boltzmann equation in the Boltzmann–Grad hydrodynamic limit [28]. In this limit, the diameter of the sphere is taken to zero, while the mass-weighted collision cross-section is kept constant (that is, $\sigma \rightarrow 0$, $\sigma^2/m = \text{const}$). However, this leads to $\rho_{sp} \rightarrow \infty$, which is physically unrealistic. As we demonstrated in Fig. 1 of [2], the atoms of noble gases have roughly constant mass density, and therefore, the constant-density hydrodynamic limit ($\sigma \rightarrow 0$, $\rho_{sp} = \text{const}$) is physically more realistic.

Expanding the mass-weighted Enskog equation in (1.4) in powers of σ , taking the constant sphere density hydrodynamic limit (instead of the conventional Boltzmann–Grad limit), and repeating the same derivation steps as are used to arrive from the Boltzmann equation to the conventional Navier–Stokes equations [28], in [2] we arrived at the following Enskog–Navier–Stokes equations in the leading order of the expansion:

$$(1.5a) \quad \frac{\partial \rho}{\partial t} + \frac{\partial}{\partial \mathbf{x}} \cdot (\rho \mathbf{u}) = 0,$$

(1.5b)

$$\frac{\partial(\rho\mathbf{u})}{\partial t} + \frac{\partial}{\partial x} \cdot (\rho\mathbf{u}\mathbf{u}^T + p\mathbf{I}) = \frac{\partial}{\partial x} \cdot \left\{ \mu \left[(1 + a_1) \left(\frac{\partial\mathbf{u}}{\partial x} + \frac{\partial\mathbf{u}^T}{\partial x} \right) - \frac{2}{3}(1 + a_2) \left(\frac{\partial}{\partial x} \cdot \mathbf{u} \right) \mathbf{I} \right] \right\},$$

(1.5c)

$$\begin{aligned} \frac{\partial(\rho\epsilon)}{\partial t} + \frac{\partial}{\partial x} \cdot ((\rho\epsilon + p)\mathbf{u}) &= \frac{15}{4} \frac{\partial}{\partial x} \cdot \left(\mu(1 + a_3) \frac{\partial\theta}{\partial x} \right) + \\ &+ \frac{\partial}{\partial x} \cdot \left\{ \mu \left[(1 + a_1) \left(\frac{\partial\mathbf{u}}{\partial x} + \frac{\partial\mathbf{u}^T}{\partial x} \right) - \frac{2}{3}(1 + a_2) \left(\frac{\partial}{\partial x} \cdot \mathbf{u} \right) \mathbf{I} \right] \mathbf{u} \right\}. \end{aligned}$$

Above, ρ , \mathbf{u} and ϵ are the density, velocity, and kinetic energy of the gas, given via the standard velocity moments

$$(1.6) \quad \rho = \int g \, dv, \quad \rho\mathbf{u} = \int v g \, dv, \quad \rho\epsilon = \frac{1}{2} \int \|v\|^2 g \, dv,$$

while θ and p are, respectively, the kinetic temperature and pressure:

$$(1.7) \quad \theta = \frac{1}{3\rho} \int \|v - \mathbf{u}\|^2 g \, dv = \frac{1}{3}(2\epsilon - \|\mathbf{u}\|^2), \quad p = \rho\theta \left(1 + \frac{4\rho}{\rho_{sp}} \right).$$

Note that, in [2], the equations in (1.5) are formulated entirely in terms of ρ , \mathbf{u} , θ and ϵ ; here we introduce the pressure variable p in (1.7) primarily for convenience – although, the expression for p in (1.7) can also be interpreted as a simplified van der Waals “equation of state” with parameters $a = 0, b = 4/\rho_{sp}$.

Observe that setting $\rho/\rho_{sp} = 0$ (which corresponds to the Boltzmann–Grad limit with $\rho_{sp} \rightarrow \infty$) in the definition of the pressure p in (1.7) reverts the latter back to its usual definition, that is, the product of the density with kinetic temperature [27, 28]. The conventional temperature T is related to θ via

$$(1.8) \quad T = \frac{\mathcal{M}}{\mathcal{R}}\theta,$$

where $\mathcal{R} = 8.314 \text{ kg m}^2/(\text{mol K s}^2)$ is the universal gas constant, \mathcal{M} is the molar mass of the gas. The viscosity μ , and the correction coefficients a_1 , a_2 and a_3 are given via

$$(1.9a) \quad \mu = \frac{5\sqrt{\pi}\rho_{sp}\sigma}{96} \sqrt{\theta}, \quad a_1 = \frac{16\rho}{5\rho_{sp}} \left(1 + \frac{4\rho}{5\rho_{sp}} \left(1 + \frac{12}{\pi} \right) \right),$$

$$(1.9b) \quad a_2 = \frac{16\rho}{5\rho_{sp}} \left(1 + \frac{4\rho}{5\rho_{sp}} \left(1 - \frac{18}{\pi} \right) \right), \quad a_3 = \frac{24\rho}{5\rho_{sp}} \left(1 + \frac{2\rho}{15\rho_{sp}} \left(9 + \frac{32}{\pi} \right) \right).$$

Again, observe that setting $\rho/\rho_{sp} = 0$, which corresponds to the Boltzmann–Grad limit with $\rho_{sp} \rightarrow \infty$, sets $a_1 = a_2 = a_3 = 0$, and reverts the equations in (1.5) back to the conventional Navier–Stokes equations [5, 27] for a monatomic gas.

The main advantage of the obtained Enskog–Navier–Stokes equations in (1.5)–(1.9) is that the gas is no longer required to be dilute, that is, average distances between the spheres are no longer required to be much larger than the diameters of the spheres themselves. As a result, the ratio ρ/ρ_{sp} is no longer presumed to be zero, and is present

in the equations as a correction term. For more details on the derivation of (1.5)–(1.9), see Section 7 of [2].

In this work, we study the properties of the shock wave transitions for the Enskog–Navier–Stokes equations in (1.5). The paper is organized as follows. In Section 2 we derive the acoustic equations and determine the corrected speed of sound for the Enskog–Navier–Stokes equations. We find that, due to the Enskog correction, the actual speed of sound in a hard sphere gas is somewhat faster than predicted by the conventional Navier–Stokes equations. In Section 3 we consider the steady one-dimensional scenario, and reduce the Enskog–Navier–Stokes dynamics to the system of two ordinary differential equations. In Section 4 we study the fixed points of the system of ordinary differential equations, which correspond to the states of the gas before and after the shock. We find that the Enskog correction tends to reduce the difference between the fixed points, and that, in particular, for a given state before the shock, the Enskog-corrected dynamics produce the post-shock state which has lower density and temperature, and higher velocity. In Section 5 we examine the heteroclinic orbit [31] which connects the fixed points, and which comprises the shock transition. We find that the Enskog-corrected model tends to increase the thickness of the shock transition in comparison with the conventional Navier–Stokes equations, particularly at transonic Mach numbers.

2. THE ACOUSTIC EQUATIONS AND THE SPEED OF SOUND

Here we compute the corrected speed of sound and the formula for the corresponding Mach number for the Enskog–Navier–Stokes equations in (1.5). Assuming homogeneity in y - and z -directions, we write the Enskog–Navier–Stokes equations as

$$(2.1a) \quad \frac{\partial \rho}{\partial t} + \frac{\partial(\rho u)}{\partial x} = 0,$$

$$(2.1b) \quad \frac{\partial(\rho u)}{\partial t} + \frac{\partial}{\partial x} (\rho u^2 + p) = \frac{4}{3} \frac{\partial}{\partial x} \left(\mu \left(1 + \frac{3}{2} a_1 - \frac{1}{2} a_2 \right) \frac{\partial u}{\partial x} \right),$$

$$(2.1c) \quad \frac{\partial(\rho \epsilon)}{\partial t} + \frac{\partial}{\partial x} ((\rho \epsilon + p)u) = \frac{15}{4} \frac{\partial}{\partial x} \left(\mu(1 + a_3) \frac{\partial \theta}{\partial x} \right) + \frac{4}{3} \frac{\partial}{\partial x} \left(\mu \left(1 + \frac{3}{2} a_1 - \frac{1}{2} a_2 \right) u \frac{\partial u}{\partial x} \right).$$

Expressing ϵ and p via (1.7), and following the same procedure as in [27], we assume $\rho = \bar{\rho} + \rho'$, $u = u'$, $\theta = \bar{\theta} + \theta'$, where the overlined terms denote the uniform background state, while the primed notations denote small fluctuations. Then, linearizing (2.1) near the background state and omitting the viscous terms, we arrive at

$$(2.2a) \quad \frac{\partial \rho'}{\partial t} + \bar{\rho} \frac{\partial u'}{\partial x} = 0,$$

$$(2.2b) \quad \bar{\rho} \frac{\partial u'}{\partial t} + \left(1 + \frac{4\bar{\rho}}{\rho_{sp}} \right) \bar{\rho} \frac{\partial \theta'}{\partial x} + \left(1 + \frac{8\bar{\rho}}{\rho_{sp}} \right) \bar{\theta} \frac{\partial \rho'}{\partial x} = 0,$$

$$(2.2c) \quad \frac{3}{2} \bar{\rho} \frac{\partial \theta'}{\partial t} + \frac{3}{2} \bar{\theta} \frac{\partial \rho'}{\partial t} + \left(\frac{5}{2} + \frac{4\bar{\rho}}{\rho_{sp}} \right) \bar{\rho} \bar{\theta} \frac{\partial u'}{\partial x} = 0.$$

The idea now is to balance the time-derivatives in (2.2c) above in the same proportions as the corresponding spatial derivatives in (2.2b), with the help of (2.2a). First, we rescale (2.2c) as

$$(2.3) \quad \left(1 + \frac{4\bar{\rho}}{\rho_{sp}}\right) \bar{\rho} \frac{\partial \theta'}{\partial t} + \left(1 + \frac{4\bar{\rho}}{\rho_{sp}}\right) \bar{\theta} \frac{\partial \rho'}{\partial t} = -\frac{2}{3} \left(1 + \frac{4\bar{\rho}}{\rho_{sp}}\right) \left(\frac{5}{2} + \frac{4\bar{\rho}}{\rho_{sp}}\right) \bar{\rho} \bar{\theta} \frac{\partial u'}{\partial x}.$$

Second, we rescale (2.2a) as

$$(2.4) \quad \frac{4\bar{\rho}}{\rho_{sp}} \bar{\theta} \frac{\partial \rho'}{\partial t} = -\frac{4\bar{\rho}}{\rho_{sp}} \bar{\rho} \bar{\theta} \frac{\partial u'}{\partial x}.$$

Adding the results together, we arrive at

$$(2.5) \quad \frac{\partial}{\partial t} \left(\left(1 + \frac{4\bar{\rho}}{\rho_{sp}}\right) \bar{\rho} \theta' + \left(1 + \frac{8\bar{\rho}}{\rho_{sp}}\right) \bar{\theta} \rho' \right) = -\frac{5}{3} \left(1 + \frac{8\bar{\rho}}{\rho_{sp}} + \frac{32\bar{\rho}^2}{5\rho_{sp}^2}\right) \bar{\rho} \bar{\theta} \frac{\partial u'}{\partial x}.$$

Differentiating in t and dividing by the product $\bar{\rho} \bar{\theta}$, we have

$$(2.6) \quad \frac{\partial^2}{\partial t^2} \left(\left(1 + \frac{8\bar{\rho}}{\rho_{sp}}\right) \frac{\rho'}{\bar{\rho}} + \left(1 + \frac{4\bar{\rho}}{\rho_{sp}}\right) \frac{\theta'}{\bar{\theta}} \right) = -\frac{5}{3} \left(1 + \frac{8\bar{\rho}}{\rho_{sp}} + \frac{32\bar{\rho}^2}{5\rho_{sp}^2}\right) \frac{\partial^2 u'}{\partial t \partial x}.$$

Now, we differentiate (2.2b) in x , arriving at

$$(2.7) \quad \frac{\partial^2}{\partial x^2} \left(\left(1 + \frac{8\bar{\rho}}{\rho_{sp}}\right) \frac{\rho'}{\bar{\rho}} + \left(1 + \frac{4\bar{\rho}}{\rho_{sp}}\right) \frac{\theta'}{\bar{\theta}} \right) = -\frac{1}{\bar{\theta}} \frac{\partial^2 u'}{\partial t \partial x}.$$

Equating the mixed derivatives in the last two equations, we obtain

$$(2.8) \quad \left[\frac{\partial^2}{\partial t^2} - \frac{5}{3} \bar{\theta} \left(1 + \frac{8\bar{\rho}}{\rho_{sp}} + \frac{32\bar{\rho}^2}{5\rho_{sp}^2}\right) \frac{\partial^2}{\partial x^2} \right] \left(\left(1 + \frac{8\bar{\rho}}{\rho_{sp}}\right) \frac{\rho'}{\bar{\rho}} + \left(1 + \frac{4\bar{\rho}}{\rho_{sp}}\right) \frac{\theta'}{\bar{\theta}} \right) = 0.$$

We arrived at the Enskog-corrected version of the acoustic equation from [27]. The speed of sound c is, obviously, given via the square root of the coefficient in front of the spatial second derivative:

$$(2.9) \quad c = \sqrt{\frac{5}{3} \bar{\theta} \left(1 + \frac{8\bar{\rho}}{\rho_{sp}} + \frac{32\bar{\rho}^2}{5\rho_{sp}^2}\right)}.$$

Setting $\bar{\rho}/\rho_{sp} = 0$, we obtain the conventional speed of sound in monatomic gases [27].

One can express the Enskog correction in the speed of sound by introducing, respectively, the conventional M and Enskog-corrected \tilde{M} Mach numbers for monatomic gases:

$$(2.10) \quad M = \frac{\bar{u}}{\sqrt{\frac{5}{3} \bar{\theta}}}, \quad \tilde{M} = \frac{\bar{u}}{\sqrt{\frac{5}{3} \bar{\theta} \left(1 + \frac{8\bar{\rho}}{\rho_{sp}} + \frac{32\bar{\rho}^2}{5\rho_{sp}^2}\right)}}.$$

As we can see, for a given velocity \bar{u} , the corrected Mach number \tilde{M} is somewhat smaller than the conventional one, because the corresponding corrected speed of sound c is somewhat larger than the conventional one. We display the relative difference between

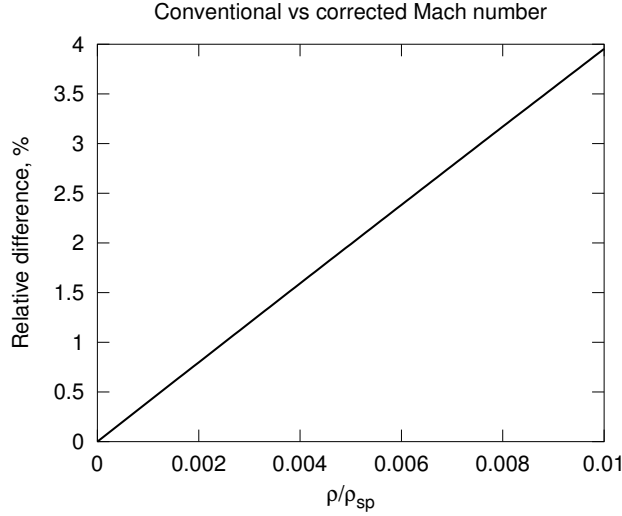


FIGURE 1. The relative difference between the conventional and corrected Mach numbers as a function of $\bar{\rho}/\rho_{sp}$.

the conventional and corrected Mach numbers as a function of $\bar{\rho}/\rho_{sp}$ in Figure 1. Observe that the relative difference between the conventional and corrected Mach numbers reaches 4% for the density ratio $\rho/\rho_{sp} = 0.01$.

3. THE STEADY ONE-DIMENSIONAL CASE: REDUCTION TO THE SYSTEM OF TWO ODES

In what follows, we examine nontrivial steady one-dimensional solutions of the Enskog–Navier–Stokes equations. The imposed conditions are quite stringent; in particular, such a solution implies that the following conditions hold:

- (1) The solution is, in effect, a one-dimensional nonlinear nondispersive wave, and
- (2) The chosen reference frame moves at an appropriate speed, so that this wave is motionless in such a reference frame.

In reality, shockwaves in gases do not behave exactly in this way, as there is always some dispersion and/or dissipation present in practical situations. However, the shockwaves behave substantially similarly to such solutions, and thus the latter are still physically meaningful. Also, as we will see below, such stringent requirements on solutions allow to reduce the system of three partial differential equations above into a system of two ordinary differential equations, which is relatively simple to examine.

Assuming uniformity in the t -direction, we simplify (2.1) above into

$$(3.1a) \quad \frac{d}{dx}(\rho u) = 0,$$

$$(3.1b) \quad \frac{d}{dx}(\rho u^2 + p) = \frac{4}{3} \frac{d}{dx} \left(\mu \left(1 + \frac{3}{2}a_1 - \frac{1}{2}a_2 \right) \frac{du}{dx} \right),$$

$$(3.1c) \quad \frac{d}{dx}((\rho\epsilon + p)u) = \frac{15}{4} \frac{d}{dx} \left(\mu(1 + a_3) \frac{d\theta}{dx} \right) + \frac{4}{3} \frac{d}{dx} \left(\mu \left(1 + \frac{3}{2}a_1 - \frac{1}{2}a_2 \right) u \frac{du}{dx} \right).$$

Integrating on both sides, we arrive at

$$(3.2a) \quad \rho u = \rho_0 u_0,$$

$$(3.2b) \quad \frac{4}{3}\mu \left(1 + \frac{3}{2}a_1 - \frac{1}{2}a_2\right) \frac{du}{dx} = (\rho u^2 + p) - (\rho_0 u_0^2 + p_0),$$

$$(3.2c) \quad \frac{15}{4}\mu(1 + a_3) \frac{d\theta}{dx} + \frac{4}{3}\mu \left(1 + \frac{3}{2}a_1 - \frac{1}{2}a_2\right) u \frac{du}{dx} = (\rho\epsilon + p)u - (\rho_0\epsilon_0 + p_0)u_0,$$

where ρ_0 , u_0 , ϵ_0 and p_0 denote the initial values of the density, velocity, kinetic energy and pressure. In particular, if the terminal, post-shock values are defined via ρ_1 , u_1 , ϵ_1 and p_1 , then it is easy to see that the corresponding Rankine–Hugoniot shock conditions are given via

$$(3.3) \quad \rho_0 u_0 = \rho_1 u_1, \quad \rho_0 u_0^2 + p_0 = \rho_1 u_1^2 + p_1, \quad \epsilon_0 + p_0/\rho_0 = \epsilon_1 + p_1/\rho_1.$$

Multiplying the second equation by u and subtracting from the third, we arrive at

$$(3.4a) \quad \rho u = \rho_0 u_0,$$

$$(3.4b) \quad \frac{4}{3}\mu \left(1 + \frac{3}{2}a_1 - \frac{1}{2}a_2\right) \frac{du}{dx} = (\rho u^2 + p) - (\rho_0 u_0^2 + p_0),$$

$$(3.4c) \quad \frac{15}{4}\mu(1 + a_3) \frac{d\theta}{dx} = \rho u(\epsilon - u^2) - \rho_0 u_0(\epsilon_0 - u_0 u) + p_0(u - u_0).$$

In what follows, we write the equations above entirely via the ρ , u , θ variables, since they are defined in a straightforward fashion by the corresponding velocity moments in (1.6) and (1.7). The kinetic energy ϵ and pressure p are expressed in terms of ρ , u , θ via (1.7). Expressing

$$(3.5) \quad u = \frac{\rho_0 u_0}{\rho}, \quad \frac{du}{dx} = -\frac{\rho_0 u_0}{\rho^2} \frac{d\rho}{dx},$$

we exclude the velocity u from the set of unknowns of the system, and arrive at

$$(3.6a) \quad \frac{4}{3}\mu \left(1 + \frac{3}{2}a_1 - \frac{1}{2}a_2\right) \frac{d\rho}{dx} = \rho^2 u_0 \left(1 - \frac{\rho_0}{\rho} - \frac{\theta_0}{u_0^2} \left(\frac{\rho\theta}{\rho_0\theta_0} - 1 + \frac{4\rho_0}{\rho_{sp}} \left(\frac{\rho^2\theta}{\rho_0^2\theta_0} - 1\right)\right)\right),$$

$$(3.6b) \quad \frac{15}{2}\mu(1 + a_3) \frac{d\theta}{dx} = \rho_0 u_0 \theta_0 \left(3 \left(\frac{\theta}{\theta_0} - 1\right) - \frac{u_0^2}{\theta_0} \left(1 - \frac{\rho_0}{\rho}\right)^2 - 2 \left(1 + \frac{4\rho_0}{\rho_{sp}}\right) \left(1 - \frac{\rho_0}{\rho}\right)\right).$$

This is a 2×2 system of ordinary differential equations, with $\rho(x)$ and $\theta(x)$ being unknown functions, and ρ_0 , u_0 and θ_0 being constant parameters.

In what follows, we look for solutions of (3.6) which approach one fixed point at $x \rightarrow -\infty$, and another, distinct, fixed point at $x \rightarrow +\infty$, with a transition in between. This approach corresponds well to what is normally observed in shockwaves traveling through a gas – typically, there is a spatially uniform state before the shock transition, and then the gas relaxes to another spatially uniform state after the shock transition.

Note that one of the fixed points of the system in (3.6) is already given via $\rho(x) = \rho_0$, $\theta(x) = \theta_0$. Thus, we first need to find other fixed points of (3.6), and then examine the orbits which connect them.

4. THE FIXED POINTS

Above, we arrived at the system (3.6) of two ODEs for ρ and θ as functions of the spatial coordinate. First, we examine the remaining fixed points of the system, in addition to the already known fixed point $\rho(x) = \rho_0$, $\theta(x) = \theta_0$.

To compute the fixed points, we set the derivatives of ρ and θ above in (3.6) to zero, and observe that both resulting equations are linear in θ . This allows us to express θ via ρ with help of the second equation in (3.6):

$$(4.1) \quad \theta = \theta_0 + \frac{1}{3} \left(1 - \frac{\rho_0}{\rho}\right) \left[u_0^2 \left(1 - \frac{\rho_0}{\rho}\right) + 2\theta_0 \left(1 + \frac{4\rho_0}{\rho_{sp}}\right) \right].$$

Next, we substitute the expression above into the first equation in (3.6), which results in following algebraic equation for ρ alone:

$$(4.2) \quad -\rho_0 u_0^2 (\rho - \rho_0) + \rho \theta_0 (\rho - \rho_0) + \frac{4}{\rho_{sp}} \rho \theta_0 (\rho - \rho_0) (\rho + \rho_0) + \frac{1}{3} \left(1 + \frac{4\rho}{\rho_{sp}}\right) \rho (\rho - \rho_0) \left(u_0^2 \left(1 - \frac{\rho_0}{\rho}\right) + 2\theta_0 \left(1 + \frac{4\rho_0}{\rho_{sp}}\right) \right) = 0.$$

Clearly, one of the solutions is $\rho = \rho_0$, which was already mentioned above. To look for a different root, we divide by $(\rho - \rho_0)$, and arrive at the quadratic equation

$$(4.3) \quad \frac{4}{\rho_{sp}} \left(u_0^2 + 5\theta_0 \left(1 + \frac{8\rho_0}{5\rho_{sp}}\right) \right) \rho^2 + \left(5\theta_0 \left(1 + \frac{4\rho_0}{\rho_{sp}}\right) + u_0^2 \left(1 - \frac{4\rho_0}{\rho_{sp}}\right) \right) \rho - 4\rho_0 u_0^2 = 0.$$

This equation has two real roots – one positive, and one negative. We, however, are interested only in the positive root, since ρ is the density and cannot be negative. The positive root of (4.3) is given via

$$(4.4) \quad \rho_1 = \frac{\rho_{sp}}{8} \frac{3 + M_0^2 \left(1 - \frac{4\rho_0}{\rho_{sp}}\right) + \frac{12\rho_0}{\rho_{sp}}}{3 + M_0^2 + \frac{24\rho_0}{5\rho_{sp}}} \left(\sqrt{1 + \frac{\rho_0}{\rho_{sp}} \frac{64M_0^2 \left(3 + M_0^2 + \frac{24\rho_0}{5\rho_{sp}}\right)}{\left(3 + M_0^2 \left(1 - \frac{4\rho_0}{\rho_{sp}}\right) + \frac{12\rho_0}{\rho_{sp}}\right)^2} - 1} \right).$$

Knowing ρ_1 , we can express u_1 and θ_1 via

$$(4.5) \quad u_1 = \frac{\rho_0 u_0}{\rho_1}, \quad \theta_1 = \theta_0 \left(1 + \frac{5}{9} \left(1 - \frac{\rho_0}{\rho_1}\right) \left(\frac{6}{5} + M_0^2 \left(1 - \frac{\rho_0}{\rho_1}\right) + \frac{24\rho_0}{5\rho_{sp}}\right)\right).$$

Combining (4.4) and (4.5) together, we can write

$$(4.6) \quad (\rho_1, u_1, \theta_1) = \mathcal{F}_{\rho_{sp}}(\rho_0, u_0, \theta_0).$$

Clearly, $\mathcal{F}_{\rho_{sp}} \circ \mathcal{F}_{\rho_{sp}} = \text{identity}$. In what follows, we will tacitly assume that (ρ_0, u_0, θ_0) corresponds to the state before the shock (that is, the one with higher velocity and lower

density and temperature), while (ρ_1, u_1, θ_1) corresponds to the state after the shock (the one with lower velocity and higher density and temperature), unless otherwise specified.

To find the conditions under which the fixed points coalesce (that is, the state before the shock is identical to the state after the shock), we equate $\rho_1 = \rho_0$ in (4.4). This yields

$$(4.7) \quad u_0^2 = \frac{5}{3} \theta_0 \left(1 + \frac{8\rho_0}{\rho_{sp}} + \frac{32\rho_0^2}{5\rho_{sp}^2} \right),$$

that is, the Enskog-corrected Mach number \tilde{M}_0 in (2.10), corresponding to ρ_0 , u_0 and θ_0 , must be equal to 1, which is to be expected.

4.1. The fixed points for the conventional Navier–Stokes equations. To obtain the fixed points for the conventional Navier–Stokes equations, we set $\rho_0/\rho_{sp} = 0$ above in (4.4) and (4.5). This yields the following, much more simple, relations

$$(4.8) \quad \rho_{1,NS} = \rho_0 \frac{4M_0^2}{M_0^2 + 3}, \quad u_{1,NS} = u_0 \frac{M_0^2 + 3}{4M_0^2}, \quad \theta_{1,NS} = \theta_0 \frac{(M_0^2 + 3)(5M_0^2 - 1)}{16M_0^2}.$$

Here we can see that the conventional Mach number cannot be less than $1/\sqrt{5}$ (otherwise, the temperature would become negative). We can also conveniently express the post-shock Mach number in terms of the pre-shock Mach number via

$$(4.9) \quad M_1^2 = \frac{3 u_{1,NS}^2}{5 \theta_{1,NS}} = \frac{M_0^2 + 3}{5M_0^2 - 1}.$$

4.2. Qualitative behavior for a small density ratio. For a small density ratio ρ_0/ρ_{sp} , we expand (4.4) and (4.5) in leading order to obtain

$$(4.10a) \quad \rho_1 \approx \rho_0 \frac{4M_0^2}{M_0^2 + 3} \left(1 - \frac{12\rho_0}{\rho_{sp}} \frac{M_0^2 + 1}{M_0^2 + 3} \right),$$

$$(4.10b) \quad u_1 \approx u_0 \frac{M_0^2 + 3}{4M_0^2} \left(1 + \frac{12\rho_0}{\rho_{sp}} \frac{M_0^2 + 1}{M_0^2 + 3} \right).$$

$$(4.10c) \quad \theta_1 \approx \theta_0 \frac{(M_0^2 + 3)(5M_0^2 - 1)}{16M_0^2} \left(1 - \frac{8\rho_0}{\rho_{sp}} \frac{5M_0^4 + 3}{(M_0^2 + 3)(5M_0^2 - 1)} \right).$$

Observe that the correction factor always reduces the difference between the pre-shock and post-shock states. Assuming that ρ_0 , u_0 and θ_0 are the values corresponding to the region before the shock (i.e. $M_0 > 1$), we conclude that the relative effect of the correction factor is weakest for $M_0 \approx 1$, and increases as $M_0 \rightarrow \infty$.

To illustrate the effect of the Enskog correction on the fixed points, in Figure 2 we show the post-shock ratios $\rho_1/\rho_{1,NS}$, $u_1/u_{1,NS}$, $T_1/T_{1,NS}$ (where we display the conventional temperature T instead of θ to provide a better understanding of the thermodynamic regime, see (1.8) for the relation between θ and T) for the given pre-shock values of ρ_0/ρ_{sp} , u_0 and T_0 of an argon-like hard sphere gas, with the physical parameters of the spheres specified as follows:

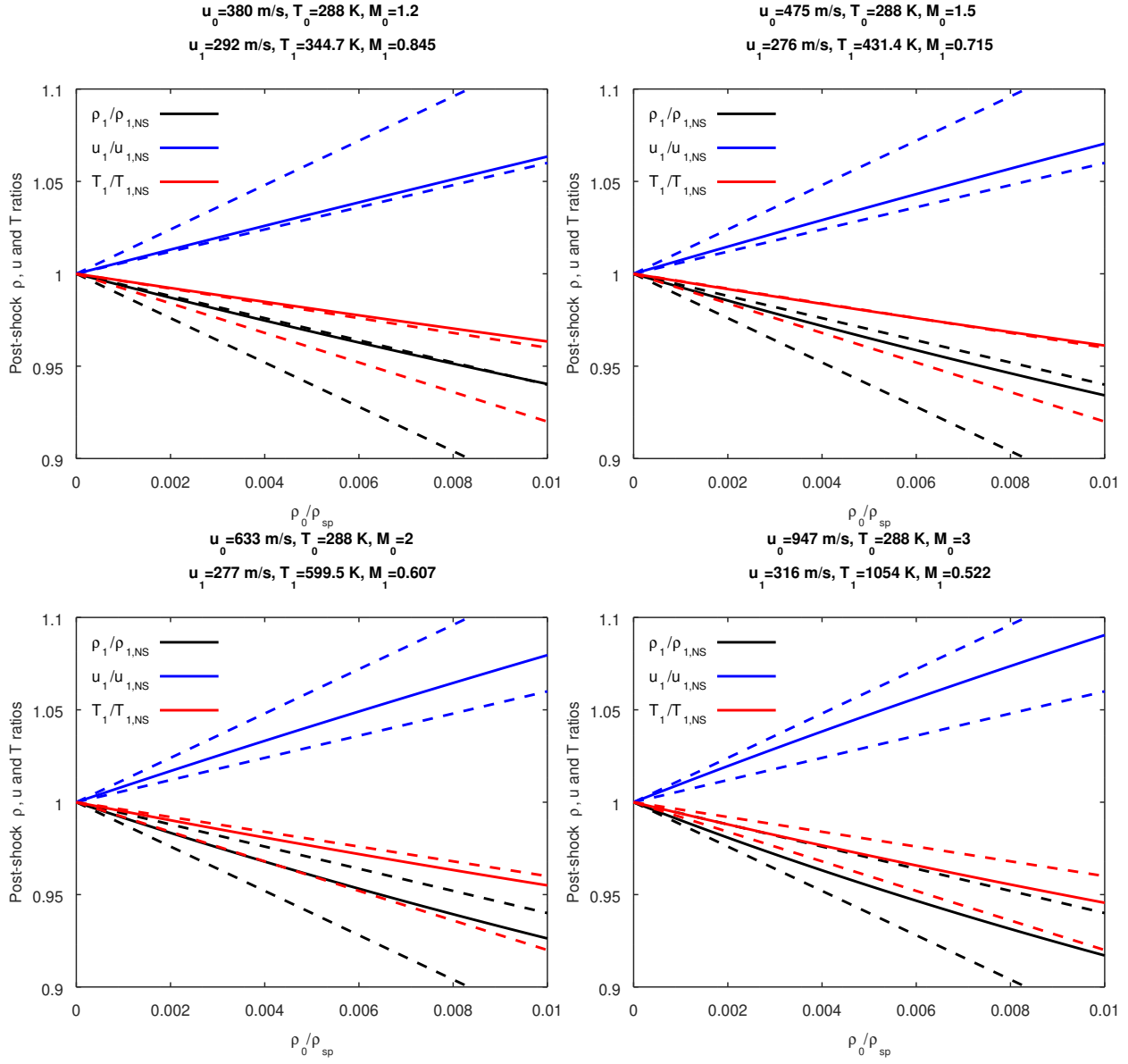


FIGURE 2. Post-shock ratios ρ/ρ_{NS} , u/u_{NS} , and T/T_{NS} for different incident Mach numbers. The pre-shock temperature is set to 288 K, and corresponds to standard conditions.

- The sphere diameter $\sigma = 3.6 \cdot 10^{-10}$ meters;
- The sphere density $\rho_{sp} = 2716$ kg/m³.

Such a sphere possesses roughly the same mass as one atom of argon, and has viscosity $\mu \approx 2.2 \cdot 10^{-5}$ kg/(m s) at $T = 288$ K, which is also similar to argon. Together with the exactly computed (via (4.4) and (4.5)) ratios, which are given as solid lines, we also plot the linearized cones given via (4.10) for minimal (1) and maximal (∞) pre-shock Mach number values as dashed lines of the same color. The pre-shock temperature is set

at $T_0 = 288$ K, while the pre-shock velocity u_0 is chosen to represent the four incident Mach number regimes, $M_0 = 1.2, 1.5, 2$ and 3 . The range of the pre-shock density values ρ_0 is chosen so that the ratio ρ_0/ρ_{sp} varies between zero and 0.01 . Observe that, for the presented range of ρ_0/ρ_{sp} , the exactly computed ratios $\rho_1/\rho_{1,NS}$, $u_1/u_{1,NS}$, $T_1/T_{1,NS}$ behave almost linearly, and generally fall within the linearized cones. We can observe that, for $\rho_0/\rho_{sp} = 0.01$, the effect of the Enskog correction varies between roughly 5% (for transonic Mach numbers) to about 10% (for supersonic Mach numbers). For the normal atmospheric pressure and temperature, the equivalent argon density is about 1.7 kg/m³, which corresponds to roughly 1% of the effect of the Enskog correction.

5. THE SHOCK TRANSITIONS

With the information about the relevant fixed points of (3.6), we can now study the transition between them. Clearly, if we accept that the state of the gas before and after the shock is modeled via (ρ_0, u_0, θ_0) and (ρ_1, u_1, θ_1) , respectively, then the corresponding shock transition must be given via the heteroclinic orbit [31] of (3.6) which connects these two fixed points.

Due to complexity of (3.6), we have to compute this heteroclinic orbit numerically. This is possible to do, with good accuracy, in the following scenario:

- One fixed point is a stable node;
- Another fixed point is a saddle node;
- The heteroclinic orbit is one of the two branches of the unstable manifold of the saddle node.

In such a case, the heteroclinic orbit will be a local attracting set for nearby orbits, while the stable-node fixed point will be a local attractor. Therefore, if we choose the initial condition sufficiently close to the saddle-node fixed point, then its orbit will shrink transversally towards the heteroclinic orbit due to the fact that the stable manifold of the saddle-node fixed point is transversal to the heteroclinic orbit, while at the same time stretching along the unstable manifold and eventually falling onto the local attractor. In other words, the accuracy of the solution will be ensured by the fact that the remaining invariant manifold of the saddle node is stable. The same idea for the computation of such a shock transition was suggested in [26] for the conventional Navier–Stokes equations. In [26], the heteroclinic orbit is referred to as the “shock curve”.

We start by introducing the nondimensional notations

$$(5.1) \quad r = \frac{\rho}{\rho_0}, \quad q = \frac{\theta}{\theta_0}, \quad \mu = \eta q^{1/2}, \quad \eta = \frac{5\sqrt{\pi}\rho_{sp}\sigma\sqrt{\theta_0}}{96}, \quad x = \frac{\eta}{\rho_0 u_0} z,$$

so that $r_0 = 1$, $q_0 = 1$. This allows us to write (3.6) in the nondimensional form

$$(5.2a) \quad \frac{dr}{dz} = F(r, q), \quad \frac{dq}{dz} = G(r, q),$$

$$(5.2b) \quad F = \frac{3}{4} \left(1 + \frac{3}{2}a_1 - \frac{1}{2}a_2 \right)^{-1} q^{-1/2} \left(r(r-1) - \frac{\theta_0}{u_0^2} r^2 \left((rq-1) + \frac{4\rho_0}{\rho_{sp}} (r^2q-1) \right) \right),$$

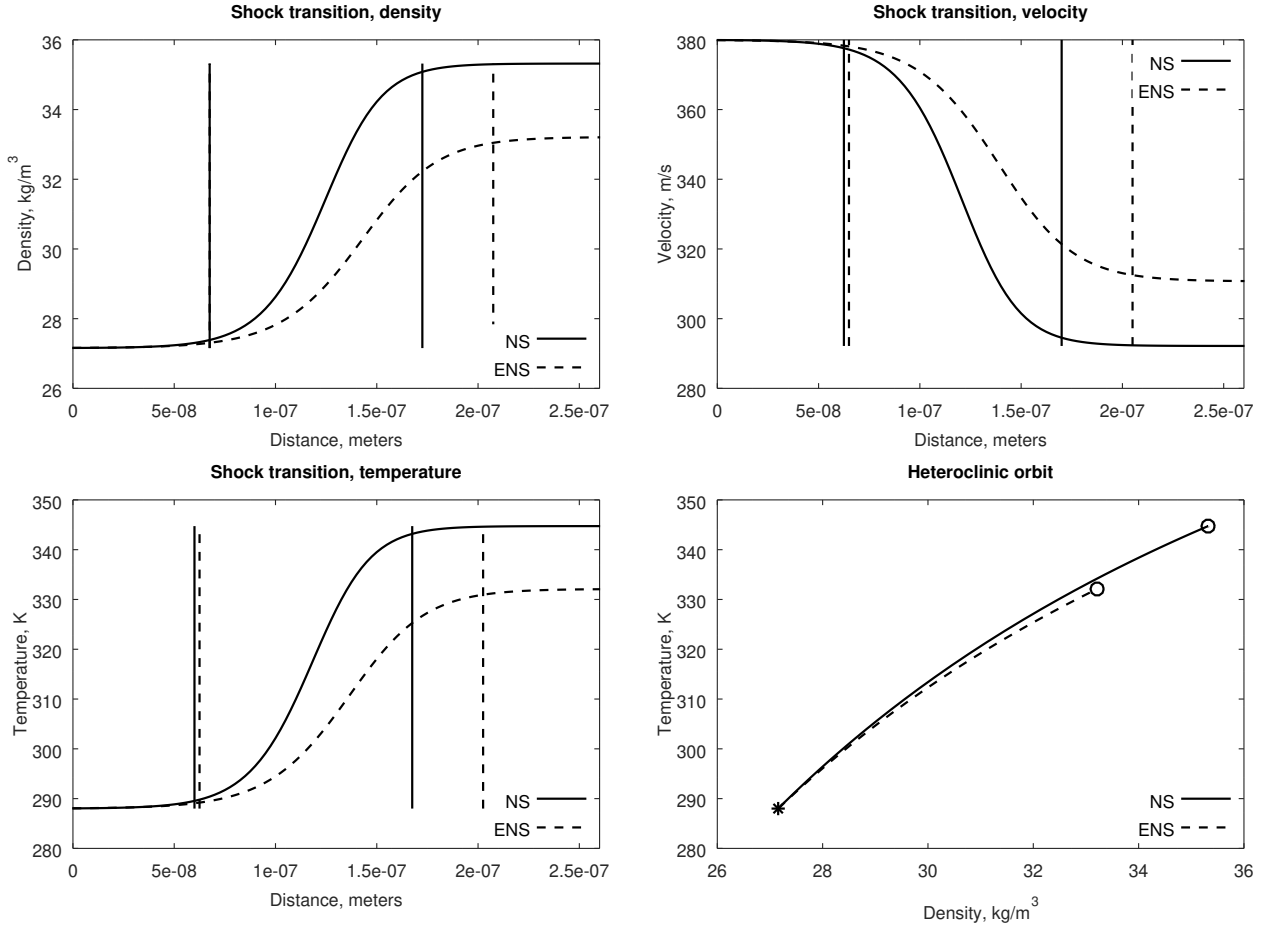


FIGURE 3. The shock transition for $\rho_0 = 27.16 \text{ kg/m}^3$, $u_0 = 380 \text{ m/s}$, $T_0 = 288 \text{ K}$, $M_0 = 1.2$. Solid line – conventional Navier–Stokes transition, dashed line – Enskog-corrected Navier–Stokes transition. The boundaries of the shock transitions are marked by the vertical lines of corresponding styles.

$$(5.2c) \quad G = \frac{2}{15}(1 + a_3)^{-1}q^{-1/2} \left(3(q - 1) - \frac{u_0^2}{\theta_0} \frac{1}{r^2} (r - 1)^2 - 2 \left(1 + \frac{4\rho_0}{\rho_{sp}} \right) \frac{1}{r} (r - 1) \right).$$

Here we observe that

$$(5.3) \quad 3a_1 - a_2 > 0, \quad a_3 > 0,$$

which means that the vector field above is smooth everywhere in the first quadrant of the (r, q) -plane.

Now, we need to determine the stability of the fixed point $(1, 1)$. This will be accomplished via the Grobman–Hartman theorem [30, 32]; if the fixed point is indeed hyperbolic, then its stability properties are the same as those of the linearized system.

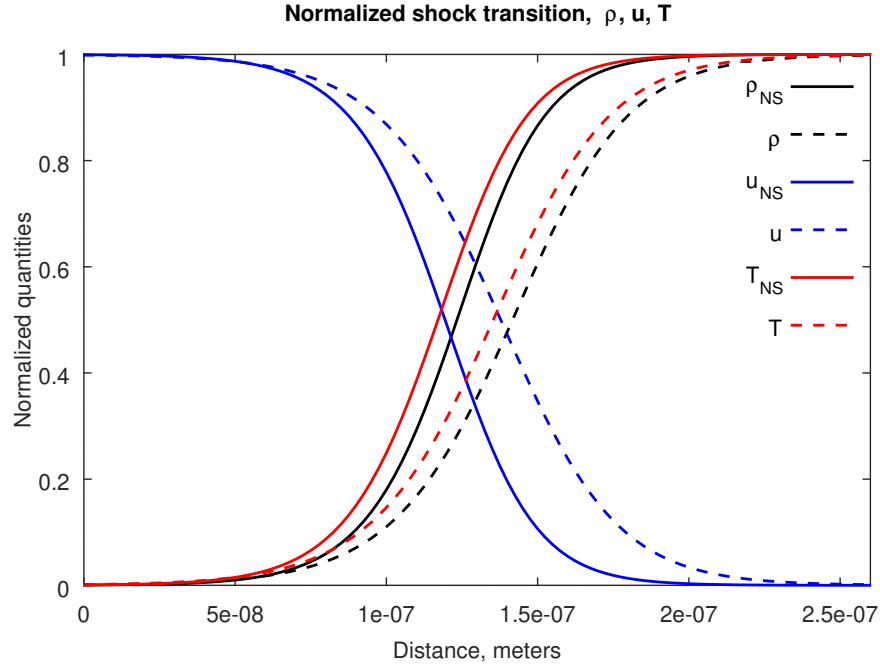


FIGURE 4. The normalized shock transition for $\rho_0 = 27.16 \text{ kg/m}^3$, $u_0 = 380 \text{ m/s}$, $T_0 = 288 \text{ K}$, $M_0 = 1.2$. Solid line – conventional Navier–Stokes transition, dashed line – Enskog-corrected Navier–Stokes transition.

For that, we compute the partial derivatives

$$(5.4a) \quad \frac{\partial F}{\partial r}(1,1) = \frac{3}{4} \left(1 + \frac{3}{2}a_1 - \frac{1}{2}a_2\right)^{-1} \left(1 - \frac{\theta_0}{u_0^2} \left(1 + \frac{8\rho_0}{\rho_{sp}}\right)\right),$$

$$(5.4b) \quad \frac{\partial F}{\partial q}(1,1) = -\frac{3}{4} \left(1 + \frac{3}{2}a_1 - \frac{1}{2}a_2\right)^{-1} \frac{\theta_0}{u_0^2} \left(1 + \frac{4\rho_0}{\rho_{sp}}\right),$$

$$(5.4c) \quad \frac{\partial G}{\partial r}(1,1) = -\frac{4}{15}(1 + a_3)^{-1} \left(1 + \frac{4\rho_0}{\rho_{sp}}\right), \quad \frac{\partial G}{\partial q}(1,1) = \frac{2}{5}(1 + a_3)^{-1},$$

where, of course, a_1 , a_2 and a_3 are evaluated for $\rho = \rho_0$. The characteristic equation is given via

$$(5.5) \quad \lambda^2 - \left(\frac{\partial F}{\partial r}(1,1) + \frac{\partial G}{\partial q}(1,1)\right) \lambda + \frac{\partial F}{\partial r}(1,1) \frac{\partial G}{\partial q}(1,1) - \frac{\partial F}{\partial q}(1,1) \frac{\partial G}{\partial r}(1,1) = 0,$$

which has roots of the same sign if

$$(5.6) \quad \frac{\partial F}{\partial r}(1,1) \frac{\partial G}{\partial q}(1,1) - \frac{\partial F}{\partial q}(1,1) \frac{\partial G}{\partial r}(1,1) > 0,$$

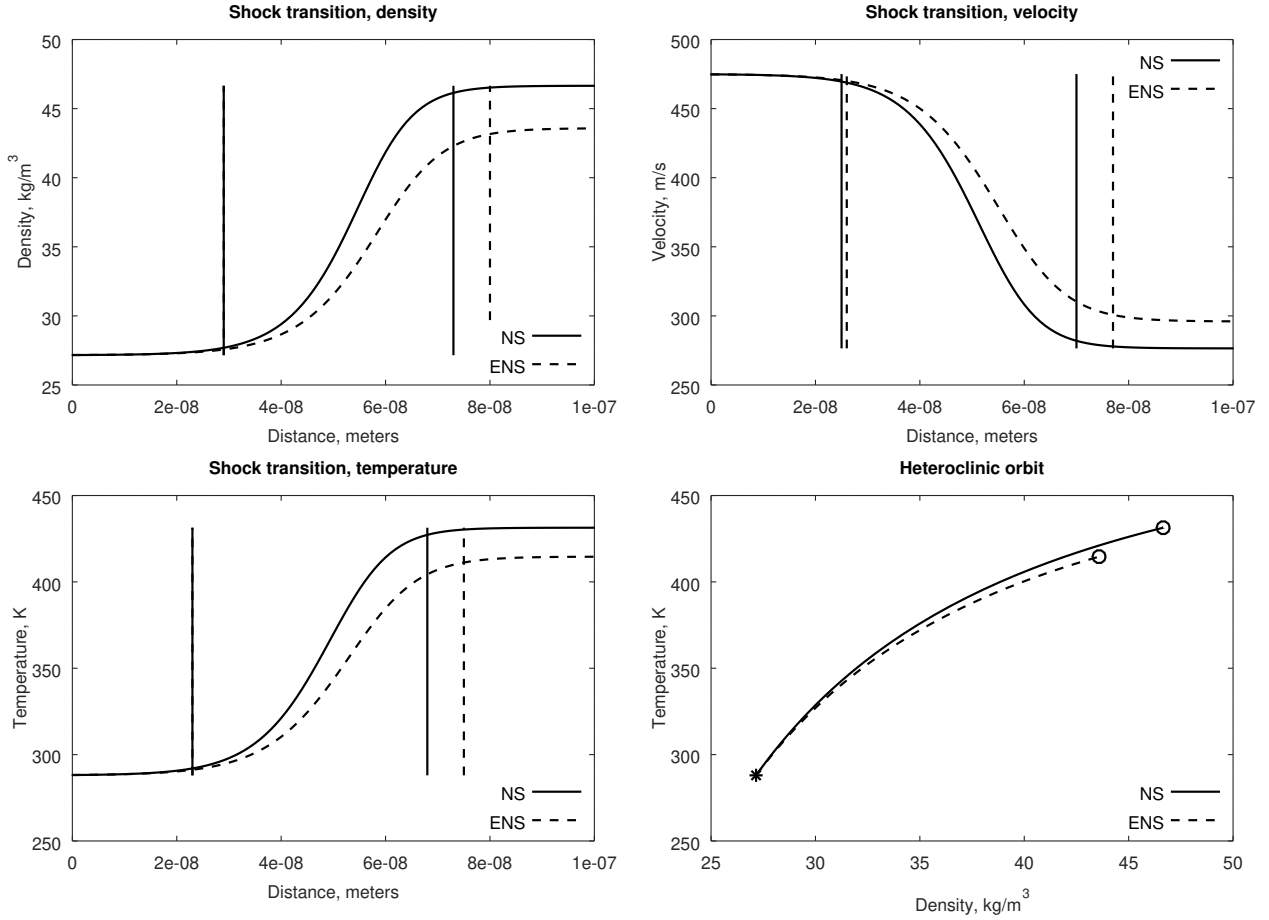


FIGURE 5. The shock transition for $\rho_0 = 27.16 \text{ kg/m}^3$, $u_0 = 475 \text{ m/s}$, $T_0 = 288 \text{ K}$, $M_0 = 1.5$. Solid line – conventional Navier–Stokes transition, dashed line – Enskog-corrected Navier–Stokes transition. The boundaries of the shock transitions are marked by the vertical lines of corresponding styles.

and roots of the opposite sign otherwise. Using the expressions above, we find that, for the roots of the same sign, we need to have

$$(5.7) \quad \frac{5}{3} \left(1 + \frac{8\rho_0}{\rho_{sp}} + \frac{32\rho_0^2}{5\rho_{sp}^2} \right) \frac{\theta_0}{u_0^2} < 1,$$

or, alternatively,

$$(5.8) \quad \tilde{M}_0 > 1.$$

Observing that for $\tilde{M}_0 > 1$ both partial derivatives $\partial F/\partial r$ and $\partial G/\partial q$ are positive, we determine that both roots are positive, which means that the pre-shock fixed point is an unstable node, and, therefore, the post-shock fixed point is a saddle. The same analysis, but for the conventional Navier–Stokes equations, is presented in Chapter 12 of [38]. Thus, in order to capture the heteroclinic orbit (and thus the shock transition), we integrate (5.2) “backwards”, that is, from the post-shock state (ρ_1, u_1, θ_1) towards the

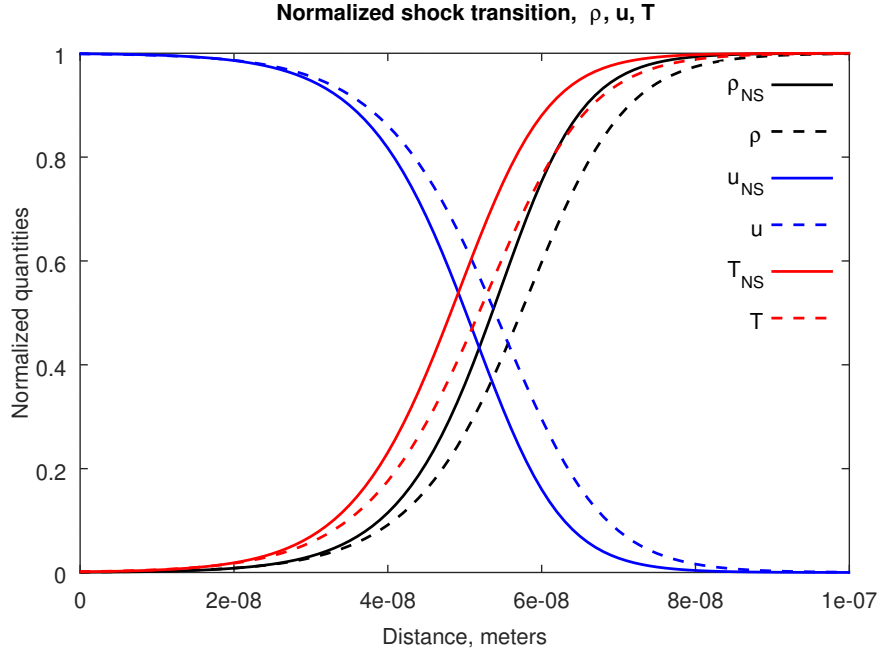


FIGURE 6. The normalized shock transition for $\rho_0 = 27.16 \text{ kg/m}^3$, $u_0 = 475 \text{ m/s}$, $T_0 = 288 \text{ K}$, $M_0 = 1.5$. Solid line – conventional Navier–Stokes transition, dashed line – Enskog-corrected Navier–Stokes transition.

pre-shock state (ρ_0, u_0, θ_0) , which effectively reverts the sign of z in (5.2), rendering the pre-shock state attracting.

In Figures 3–10 we compute the shock transitions, as described above, for ρ , u , and the conventional temperature T (see (1.8) for the relation between θ and T) for the same argon-like hard sphere gas as above. To numerically capture the heteroclinic orbit in (5.2), we perturb the post-shock fixed point by $10^{-6}\%$ in the direction of the pre-shock fixed point, and then use the *lsode* routine [33] of the Octave software [20] to carry out the numerical integration. We compute the spatial “thickness” of the shock transition as the length on which 95% of the transition occurs, situated symmetrically between the fixed points – that is, the transition starts when 2.5% of the distance between the fixed points is covered, and ends when 2.5% of the distance remains. The start and end of each transition are marked on plots by vertical lines.

In all cases, we set $T_0 = 288 \text{ K}$ and $\rho_0 = 27.16 \text{ kg/m}^3$ (so that $\rho_0/\rho_{sp} = 0.01$), and vary u_0 to achieve different incident Mach numbers. This set-up corresponds to a moderately dense gas – given that, at the sea-level pressure, the density of argon is about 1.7 kg/m^3 , the equivalent density in our set-up is roughly 16 Earth atmospheres. This is a physically realistic scenario – for example, the equivalent density for the same gas in the Cytherean atmosphere corresponds to the altitude of about 20–30 kilometers above surface, while much greater densities can be achieved in the respective atmospheres of the four gas giants of the Solar system. Moreover, the density of the gaseous part of a propellant in the combustion chamber of a rocket engine can also be of the same order of magnitude.

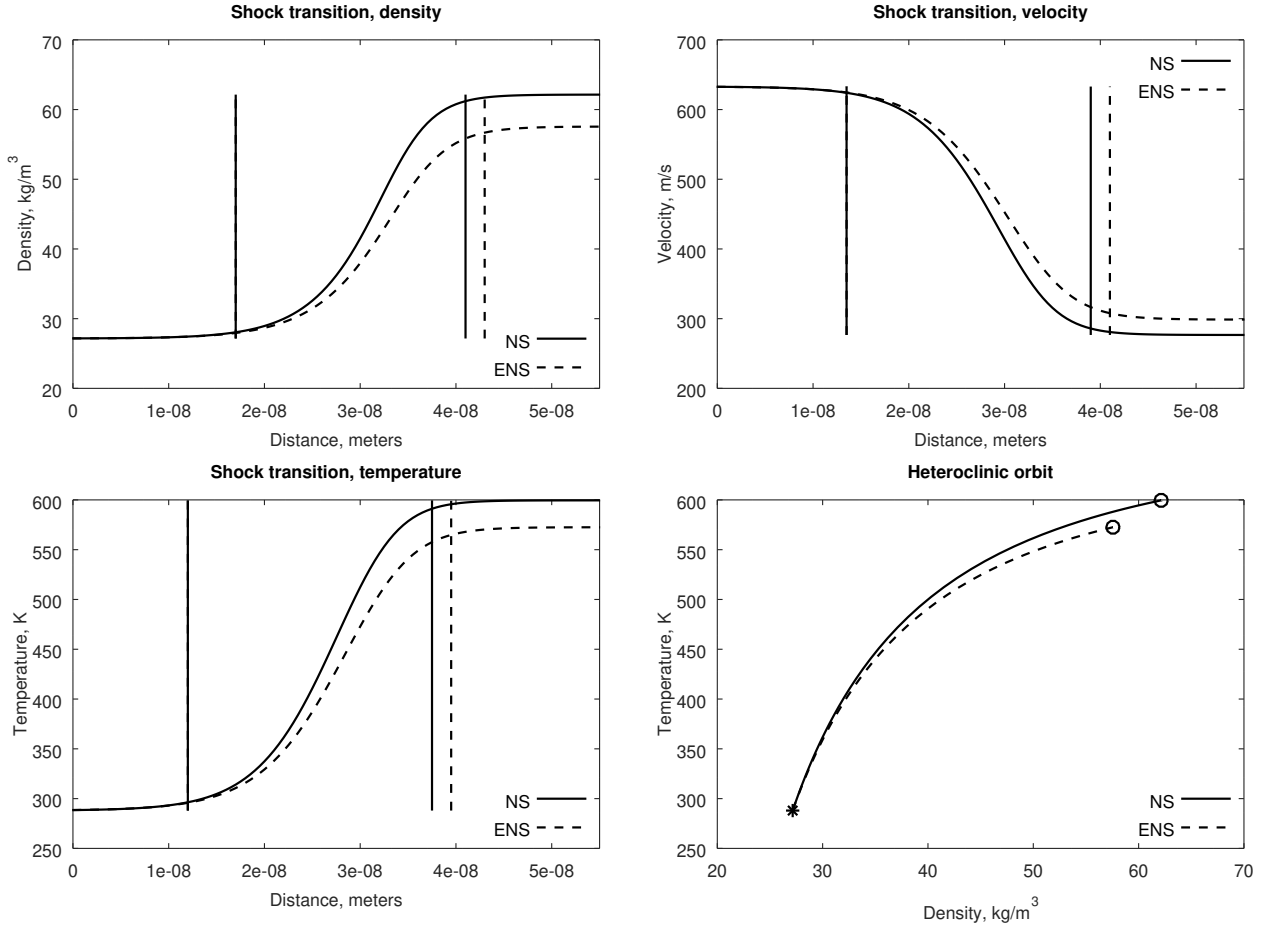


FIGURE 7. The shock transition for $\rho_0 = 27.16 \text{ kg/m}^3$, $u_0 = 633 \text{ m/s}$, $T_0 = 288 \text{ K}$, $M_0 = 2$. Solid line – conventional Navier–Stokes transition, dashed line – Enskog-corrected Navier–Stokes transition. The boundaries of the shock transitions are marked by the vertical lines of corresponding styles.

In Figures 3 and 4 we compute the shock transition for $u_0 = 380 \text{ m/s}$, or $M_0 = 1.2$. Figure 3 shows the transitions in density, velocity and temperature separately in their respective physical units, while in Figure 4 we normalize all transitions so that they vary between 0 and 1, and overlay them on the same plot. In Figure 3, we also display the heteroclinic orbit between the pre-shock and post-shock fixed points in the (ρ, T) -phase plane. Observe that, apart from the significant difference between the post-shock states for the Navier–Stokes and Enskog-corrected Navier–Stokes dynamics (which was already predicted in the previous section), there is another interesting effect of the Enskog correction – the transition between the pre-shock and post-shock states for the Enskog-corrected dynamics is longer and smoother than that for the conventional Navier–Stokes equations, so that the “thickness” of the shock is greater. We note that a similar behavior was observed in [29], which was attributed to an additional proposed mass-diffusion effect in gases [9–11, 16, 18, 19, 29]. We do not, however, insist that what we observe here

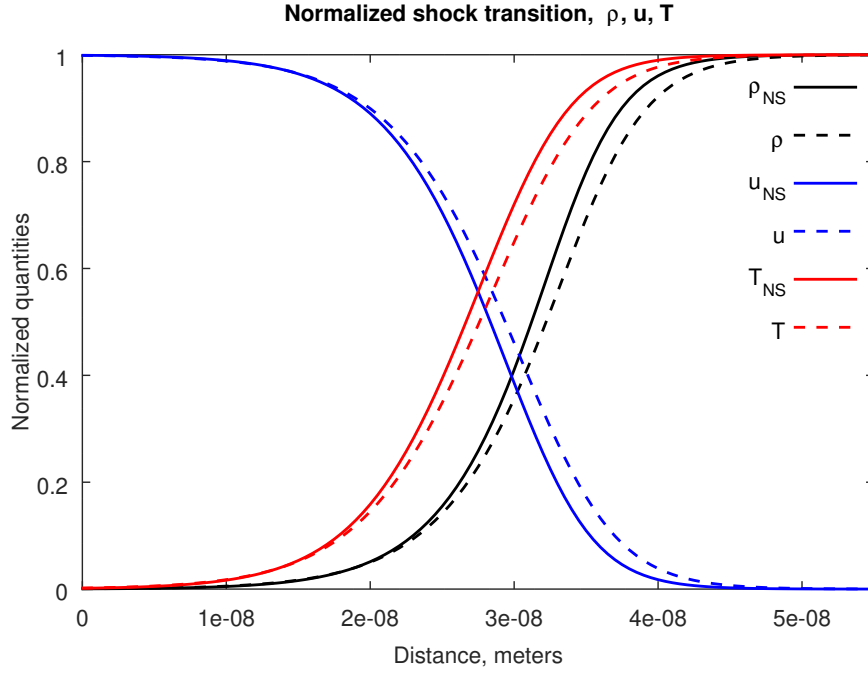


FIGURE 8. The normalized shock transition for $\rho_0 = 27.16 \text{ kg/m}^3$, $u_0 = 633 \text{ m/s}$, $T_0 = 288 \text{ K}$, $M_0 = 2$. Solid line – conventional Navier–Stokes transition, dashed line – Enskog-corrected Navier–Stokes transition.

and what was observed in [29] is necessarily the same effect, but merely point out the qualitative similarity. Also, observe that the heteroclinic orbit in the (ρ, T) -phase plane, shown in Figure 3, is close to a straight line (albeit slightly concave), which means that the density and temperature shock transitions occur almost synchronously, with temperature slightly preceding the density (also see Figure 4 with overlaid normalized plots).

In Figures 5 and 6 we compute the shock transition for $u_0 = 475 \text{ m/s}$, or $M_0 = 1.5$. Figure 5 shows the transitions in density, velocity and temperature separately in their respective physical units, while in Figure 6 we normalize all transitions so that they vary between 0 and 1, and overlay them on the same plot. In Figure 5, we also display the heteroclinic orbit between the pre-shock and post-shock fixed points in the (ρ, T) -phase plane. Here, observe that the relative difference of the thickness of the shock transition between the conventional Navier–Stokes equations and the Enskog-corrected dynamics diminishes somewhat in comparison to the previous scenario with $M_0 = 1.2$. At the same time, the heteroclinic orbit in the (ρ, T) -phase plane, shown in Figure 5, becomes more concave, which means that the temperature shock transition precedes the density shock transition a little more, relative to the overall thickness of the shock, than in the previous scenario with $M_0 = 1.2$ (this can also be observed in Figure 6 with overlaid normalized plots).

In Figures 7 and 8 we compute the shock transition for $u_0 = 633 \text{ m/s}$, or $M_0 = 2$. Unlike the two previous scenarios with $M_0 = 1.2$ and $M_0 = 1.5$, which could both be qualified as transonic or borderline transonic/supersonic, this is a strongly supersonic

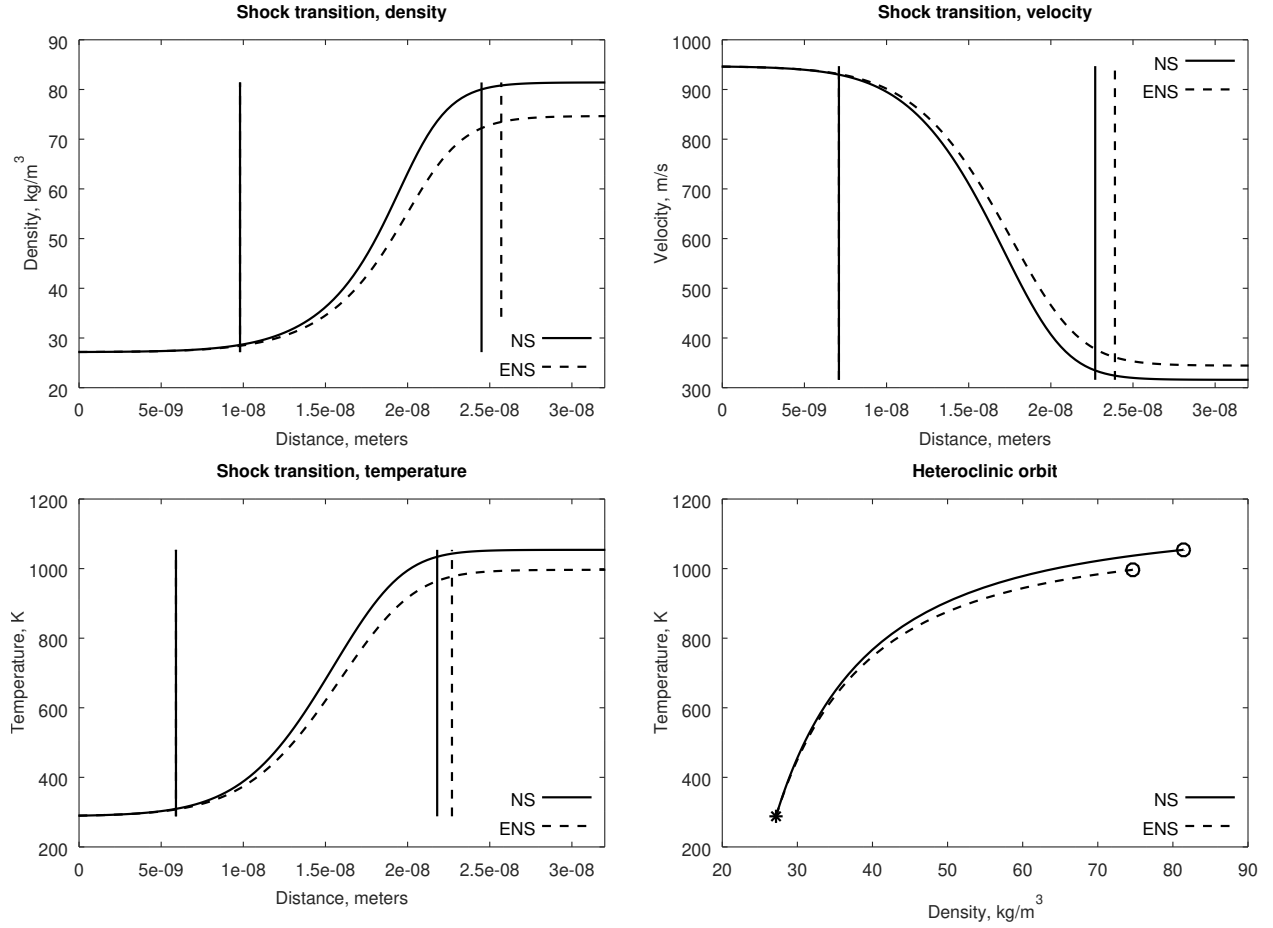


FIGURE 9. The shock transition for $\rho_0 = 27.16 \text{ kg/m}^3$, $u_0 = 947 \text{ m/s}$, $T_0 = 288 \text{ K}$, $M_0 = 3$. Solid line – conventional Navier–Stokes transition, dashed line – Enskog-corrected Navier–Stokes transition. The boundaries of the shock transitions are marked by the vertical lines of corresponding styles.

scenario, where the speed of the shock wave is roughly twice the speed of sound in the unperturbed gas in the pre-shock zone. As before, we present two separate figures, with Figure 7 showing the transitions in density, velocity and temperature separately in their respective physical units, while Figure 8 displaying the normalized transitions, overlaid on the same plot. In Figure 7, we also display the heteroclinic orbit between the pre-shock and post-shock fixed points in the (ρ, T) -phase plane. Here, observe that the earlier observed shock thickness trend continues – the relative difference of the thickness of the shock transition between the conventional Navier–Stokes equations and the Enskog-corrected dynamics is smaller than that for both previously examined Mach numbers, $M_0 = 1.2$ and $M_0 = 1.5$. The heteroclinic orbit in the (ρ, T) -phase plane, shown in Figure 7, becomes even more concave in comparison with $M_0 = 1.5$, which results in the temperature shock transition preceding the density shock transition even more, relative to the thickness of the shock itself, than in the previous scenario with $M_0 = 1.5$. The

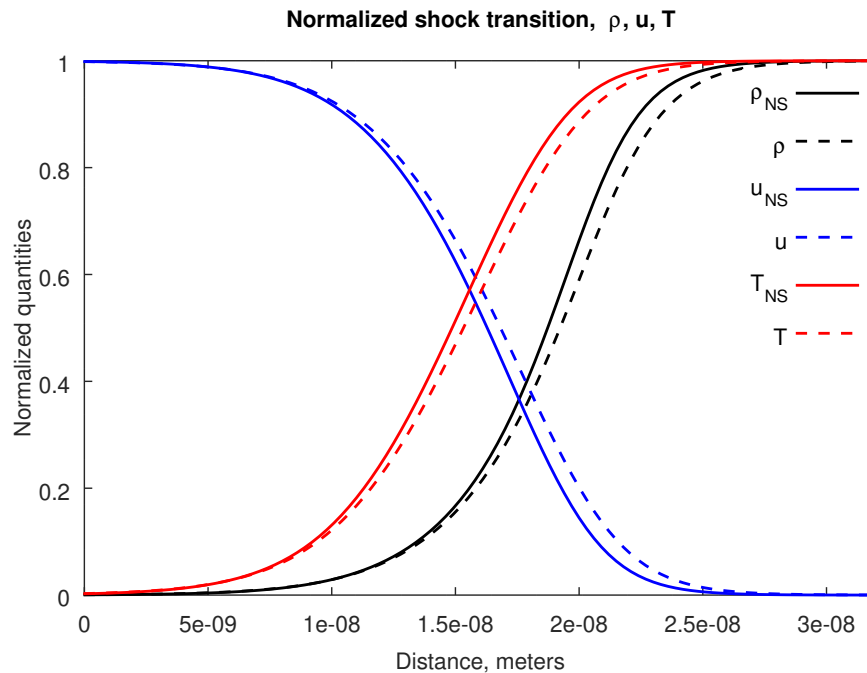


FIGURE 10. The normalized shock transition for $\rho_0 = 27.16 \text{ kg/m}^3$, $u_0 = 947 \text{ m/s}$, $T_0 = 288 \text{ K}$, $M_0 = 3$. Solid line – conventional Navier–Stokes transition, dashed line – Enskog-corrected Navier–Stokes transition.

normalized plots in Figure 8 confirm the shift between the density and temperature shock transition.

In Figures 9 and 10 we compute the shock transition for $u_0 = 947 \text{ m/s}$, or $M_0 = 3$. Like the previous scenario with $M_0 = 2$, this is also a strongly supersonic scenario, where the speed of the shock wave is roughly thrice the speed of sound in the unperturbed gas in the pre-shock zone. As before, we present two separate figures, with Figure 9 showing the transitions in density, velocity and temperature separately in their respective physical units, while Figure 10 displaying the normalized transitions, overlaid on the same plot. In Figure 9, we also display the heteroclinic orbit between the pre-shock and post-shock fixed points in the (ρ, T) -phase plane. Here, observe that the relative difference in shock thicknesses between the conventional Navier–Stokes equations and the Enskog-corrected dynamics is roughly the same as for the previous scenario with $M_0 = 2$ regime. The heteroclinic orbit in the (ρ, T) -phase plane, shown in Figure 9, is more concave than the one in the $M_0 = 2$ regime, and, as a result, the temperature shock transition precedes the density shock transition even more, relative to the thickness of the shock itself. The shift between the density and temperature shock transitions is visible on the normalized plots in Figure 10, for both the conventional Navier–Stokes and Enskog-corrected dynamics.

We summarize the shock transition thicknesses and magnitudes in Tables 1 and 2, respectively. The tables generally confirm the trends observed in the plots – the relative impact of the Enskog-corrected terms is greatest at the low Mach numbers, where the difference in transition thicknesses can reach as much as 30%. Interestingly, there is

	$M_0 = 1.2$			$M_0 = 1.5$		
	ρ	u	T	ρ	u	T
NS	$1.05 \cdot 10^{-7}$	$1.075 \cdot 10^{-7}$	$1.075 \cdot 10^{-7}$	$4.4 \cdot 10^{-8}$	$4.5 \cdot 10^{-8}$	$4.5 \cdot 10^{-8}$
ENS	$1.4 \cdot 10^{-7}$	$1.4 \cdot 10^{-7}$	$1.4 \cdot 10^{-7}$	$5.1 \cdot 10^{-8}$	$5.1 \cdot 10^{-8}$	$5.2 \cdot 10^{-8}$
Diff.	33%	30%	30%	16%	13%	16%
	$M_0 = 2$			$M_0 = 3$		
	ρ	u	T	ρ	u	T
NS	$2.4 \cdot 10^{-8}$	$2.55 \cdot 10^{-8}$	$2.55 \cdot 10^{-8}$	$1.47 \cdot 10^{-8}$	$1.56 \cdot 10^{-8}$	$1.59 \cdot 10^{-8}$
ENS	$2.6 \cdot 10^{-8}$	$2.75 \cdot 10^{-8}$	$2.75 \cdot 10^{-8}$	$1.59 \cdot 10^{-8}$	$1.68 \cdot 10^{-8}$	$1.68 \cdot 10^{-8}$
Diff.	8%	8%	8%	8%	8%	6%

TABLE 1. Thickness of shock transitions (meters) for all studied scenarios, as well as their relative differences in %.

	$M_0 = 1.2$			$M_0 = 1.5$		
	$\Delta\rho, \text{kg/m}^3$	$\Delta u, \text{m/s}$	$\Delta T, \text{K}$	$\Delta\rho, \text{kg/m}^3$	$\Delta u, \text{m/s}$	$\Delta T, \text{K}$
NS	8.164	87.83	56.73	19.5	198.5	143.4
ENS	6.057	69.3	44.11	16.43	179	126.6
Diff.	26%	21%	22%	16%	10%	12%
	$M_0 = 2$			$M_0 = 3$		
	$\Delta\rho, \text{kg/m}^3$	$\Delta u, \text{m/s}$	$\Delta T, \text{K}$	$\Delta\rho, \text{kg/m}^3$	$\Delta u, \text{m/s}$	$\Delta T, \text{K}$
NS	34.99	356.4	311.5	54.26	631.1	765.9
ENS	30.41	334.4	284.5	47.51	602.6	708.6
Diff.	13%	6%	9%	12%	5%	7%

TABLE 2. Magnitudes of shock transitions for all studied scenarios, as well as their relative differences in %.

not much of a relative difference between $M = 2$ and $M = 3$ scenarios – the relative difference in transition thicknesses in both cases is around 8%.

Here, we feel compelled to point out that the results in Table 2 do not contradict the results in Figure 2 (although it may seem so at a glance). Note that the plots in Figure 2 show the relative effect of the Enskog correction on the post-shock state itself, while the results in Table 2 show its effect on the *transition* between the pre-shock and post-shock state. So, while the relative difference in post-shock states grows with the Mach number (this trend is shown in Figure 2), the relative differences in shock transitions are more prominent at low Mach numbers (as follows from Table 2).

6. SUMMARY

In the present work we study the effect of the Enskog correction on the steady shock transitions in the supersonic flow of a hard sphere gas, modeled via the Enskog–Navier–Stokes equations [2]. First, we find that the Enskog-corrected speed of sound is somewhat larger than the conventional speed of sound, and weakly depends on the density of the gas in addition to its temperature. We then look for one-dimensional solutions in

the form of nondispersive waves, which travel in a fixed direction at a constant speed. Equating the speed of the reference frame to the speed of such a wave allows to reduce the Enskog–Navier–Stokes equations into a system of two ordinary differential equations for a spatial variable. Observing that a shock solution should asymptotically approach two distinct uniform gas states before and after the shock transition, we conclude that the shock transitions are, in fact, the heteroclinic orbits which connect distinct fixed points of this system. We then compute the fixed points of the system exactly, and examine the heteroclinic orbits numerically. Generally, we find that the Enskog correction affects the shock transition in two different ways. First, the Enskog correction leads to an overall weaker shock magnitude in comparison with the conventional Navier–Stokes equations (that is, for the same pre-shock state, the post-shock state has lower density and temperature, and higher velocity). Second, the Enskog correction increases the spatial thickness of the shock transition, making the shock wave “smoother”. These effects are relatively more prominent at low Mach numbers, and appear to be similar to what was observed in [29].

Acknowledgment. The author thanks Gregor Kovačič for useful discussions. The work was supported by the Office of Naval Research grant N00014-15-1-2036, and by the Simons Foundation grant #636144.

REFERENCES

- [1] R.V. Abramov. Diffusive Boltzmann equation, its fluid dynamics, Couette flow and Knudsen layers. *Physica A*, 484:532–557, 2017.
- [2] R.V. Abramov. The random gas of hard spheres. *J*, 2(2):162–205, 2019.
- [3] R.V. Abramov and J.T. Otto. Nonequilibrium diffusive gas dynamics: Poiseuille microflow. *Physica D*, 371:13–27, 2018.
- [4] D. Applebaum. *Lévy Processes and Stochastic Calculus*. Number 116 in Cambridge Studies in Advanced Mathematics. Cambridge University Press, 2nd edition, 2009.
- [5] G.K. Batchelor. *An Introduction to Fluid Dynamics*. Cambridge University Press, New York, 2000.
- [6] N.N. Bogoliubov. Kinetic equations. *J. Exp. Theor. Phys.*, 16(8):691–702, 1946.
- [7] L. Boltzmann. Weitere Studien über das Wärmegleichgewicht unter Gasmolekülen. *Sitz.-Ber. Kais. Akad. Wiss. (II)*, 66:275–370, 1872.
- [8] M. Born and H.S. Green. A general kinetic theory of liquids I: The molecular distribution functions. *Proc. Roy. Soc. A*, 188:10–18, 1946.
- [9] H. Brenner. Kinematics of volume transport. *Physica A*, 349:11–59, 2005.
- [10] H. Brenner. Navier-Stokes revisited. *Physica A*, 349:60–132, 2005.
- [11] H. Brenner. Fluid mechanics revisited. *Physica A*, 370:190–224, 2006.
- [12] C. Cercignani. *Theory and Application of the Boltzmann Equation*. Elsevier Science, New York, 1975.
- [13] C. Cercignani. The Boltzmann equation and its applications. In *Applied Mathematical Sciences*, volume 67. Springer, New York, 1988.
- [14] C. Cercignani, R. Illner, and M. Pulvirenti. The mathematical theory of dilute gases. In *Applied Mathematical Sciences*, volume 106. Springer-Verlag, 1994.
- [15] P. Courrège. Sur la forme intégral-différentielle des opérateurs de C_k^∞ dans C satisfaisant au principe du maximum. *Séminaire BreLOT-Choquet-Deny. Théorie du potentiel*, 10(1):1–38, 1965/66.
- [16] S.K. Dadzie and J.M. Reese. Spatial stochasticity and non-continuum effects in gas flows. *Phys. Lett. A*, 376:967–972, 2012.
- [17] D.J. Daley and D. Vere-Jones. *An Introduction to the Theory of Point Processes. Volume I: Elementary Theory and Methods*. Springer, 2nd edition, 2003.

- [18] N. Dongari, R. Sambasivam, and F. Durst. Extended Navier-Stokes equations and treatments of micro-channel gas flows. *J. Fluid Sci. Tech.*, 4(2):454–467, 2009.
- [19] F. Durst, J. Gomes, and R. Sambasivam. Thermofluidynamics: Do we solve the right kind of equations? In *Proceedings of the International Symposium on Turbulence, Heat and Mass Transfer*, pages 3–18, Dubrovnik, Croatia, 2006.
- [20] J.W. Eaton, D. Bateman, S. Hauberg, and R. Wehbring. *GNU Octave version 4.0.0 manual: a high-level interactive language for numerical computations*. 2015.
- [21] D. Enskog. Kinetische Theorie der Wärmeleitung, Reibung und Selbstdiffusion in gewissen verdichteten Gasen und Flüssigkeiten. *Kungl. Svenska Vet.-Ak. Handl.*, 63(4):3–44, 1922.
- [22] W. Feller. *An Introduction to Probability Theory and its Applications, Volume 1*. Wiley, New York, second edition, 1957.
- [23] W. Feller. *An Introduction to Probability Theory and its Applications, Volume 2*. Wiley, New York, second edition, 1971.
- [24] A. Frezzotti. Molecular dynamics and Enskog theory calculation of one dimensional problems in the dynamics of dense gases. *Physica A*, 240:202–211, 1997.
- [25] A. Frezzotti. Molecular dynamics and Enskog theory calculation of shock profiles in a dense hard sphere gas. *Computers Math. Applic.*, 35(1/2):103–112, 1998.
- [26] D. Gilbarg and D. Paolucci. The structure of shock waves in the continuum theory of fluids. *Indiana Univ. Math. J.*, 2(4):617–642, 1953.
- [27] F. Golse. *The Boltzmann Equation and its Hydrodynamic Limits*, volume 2 of *Handbook of Differential Equations: Evolutionary Equations*, chapter 3, pages 159–301. Elsevier, 2005.
- [28] H. Grad. On the kinetic theory of rarefied gases. *Comm. Pure Appl. Math.*, 2(4):331–407, 1949.
- [29] C.J. Greenshields and J.M. Reese. The structure of shock waves as a test of Brenner’s modifications to the Navier-Stokes equations. *J. Fluid. Mech.*, 580:407–429, 2007.
- [30] D.M. Grobman. Homeomorphism of systems of differential equations. *Dokl. Akad. Nauk SSSR*, 128:880–881, 1959.
- [31] J. Guckenheimer and P. Holmes. *Nonlinear Oscillations, Dynamical Systems, and Bifurcations of Vector Fields*, volume 42 of *Applied Mathematical Sciences*. Springer, 2002.
- [32] P. Hartman. A lemma in the theory of structural stability of differential equations. *Proc. Amer. Math. Soc.*, 11(4):610–620, 1960.
- [33] A.C. Hindmarsh. ODEPACK: A systematized collection of ODE solvers. In R.S. Stepleman et al., editor, *Scientific Computing*, pages 55–64. North-Holland, Amsterdam, 1983. (vol. 1 of IMACS Transactions on Scientific Computation).
- [34] J.O. Hirschfelder, C.F. Curtiss, and R.B. Bird. *The Molecular Theory of Gases and Liquids*. Wiley, 1964.
- [35] J.G. Kirkwood. The statistical mechanical theory of transport processes I: General theory. *J. Chem. Phys.*, 14:180–201, 1946.
- [36] Yu.L. Klimontovich. The unified description of kinetic and hydrodynamic processes in gases and plasmas. *Phys. Lett. A*, 170:434–438, 1992.
- [37] M. Lachowicz. On the hydrodynamic limit of the Enskog equation. *Publ. RIMS, Kyoto Univ.*, 34:191–210, 1998.
- [38] I. Müller and T. Ruggeri. *Rational Extended Thermodynamics*, volume 37 of *Springer Tracts in Natural Philosophy*. Springer, 2nd edition, 1998.
- [39] F. Papangelou. Integrability of expected increments of point processes and a related random change of scale. *Trans. Amer. Math. Soc.*, 165:483–506, 1972.
- [40] Yu.V. Sheretov. On a regularization of the Boltzmann equation consistent with integral conservation laws. In *Application of functional analysis in approximation theory*, volume 23, pages 77–92. Tver’ University Press, 2002.
- [41] H. Struchtrup and M. Torrilhon. Regularization of Grad’s 13-moment equations: Derivation and linear analysis. *Phys. Fluids*, 15:2668–2680, 2003.